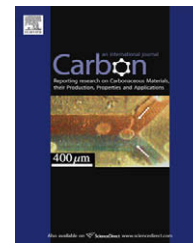


available at [www.sciencedirect.com](http://www.sciencedirect.com)journal homepage: [www.elsevier.com/locate/carbon](http://www.elsevier.com/locate/carbon)

# Mass production of aligned carbon nanotube arrays by fluidized bed catalytic chemical vapor deposition

Qiang Zhang<sup>1</sup>, Meng-Qiang Zhao, Jia-Qi Huang, Jing-Qi Nie, Fei Wei\*

Beijing Key Laboratory of Green Chemical Reaction Engineering and Technology, Department of Chemical Engineering, Tsinghua University, Beijing 100084, China

## ARTICLE INFO

### Article history:

Received 26 October 2009

Accepted 23 November 2009

Available online 26 November 2009

## ABSTRACT

A parametric study investigating the impacts of loading amount of active phase, growth temperature, H<sub>2</sub> reduction, space velocity, and apparent gas velocity on the intercalated growth of vertically aligned carbon nanotube (CNT) arrays among lamellar catalyst was performed. A series of Fe/Mo/vermiculite catalysts with Fe/vermiculite ratio of 0.0075–0.300 were tested. Metal particles were dispersed among the layers of vermiculite after H<sub>2</sub> reduction. Uniform catalyst particles, with a size of 10–20 nm and a density of  $8.5 \times 10^{14} \text{ m}^{-2}$ , were formed among the vermiculite layers at 650 °C. CNTs with high density synchronously grew into arrays among the vermiculites. With the increasing growth temperature, the alignment of CNTs intercalated among vermiculites became worse. Moreover, intercalated CNTs were synthesized among vermiculite layers in various flow regimes. The as-grown particles were with a size of 1–2 mm when the fluidized bed reactor was operated in particulate fluidization and bubbling fluidization, while the size of the as-grown products decreased obviously when they grown in the turbulent fluidized bed. Based on the understanding of the various parameters investigated, 3.0 kg/h of CNT arrays were mass produced in a pilot plant fluidized bed reactor.

© 2009 Elsevier Ltd. All rights reserved.

## 1. Introduction

Carbon nanotubes (CNTs) have become one of the most famous nanocarbon. Various potential commercial applications have been found, including engineering materials to enhance the electrical and electrostatic properties or tenacity of polymers, metals, cement, and coatings [1,2]; catalyst for oxidative dehydrogenation [3–6]; catalysis carriers for noble metals in hydrogenation, Fischer–Tropsch synthesis, and others [3,7,8]; energy conversion components of supercapacitors, fuel cells or lithium ion secondary batteries [9–12]; field emission display [13,14]; buckypaper [15]; transparent conductive film [16]; sensors, and electronics, devices [17], and so on. Some applications have been achieved on the basis of the mass production of multi-walled CNTs (MWCNTs) or single-

walled CNTs (SWCNTs), which is the first step for those fascinating applications. Recently, vertically aligned CNT (VACNT) arrays, with the advantages of good orientation, large aspect ratio, and high purity, are attractive because of their wide potential applications, i.e. in field emission devices, anisotropic conductive materials, membrane filtration materials, the super springs, filaments, super strong fibers, nano-brushes, sensors, and so on [14,18–21]. However, based on the current worldwide CNT market status, some obstacles appeared such as high prices (10 \$/g) and poor availability (around 1 kg/year). Even in the literature, the best yields of MWCNT arrays were just 1.0 g/h and 200 g/h for the synthesis on a flat quartz plate as substrate [22] and on spherical substrates [23], respectively. Compared with agglomerated CNTs, it is critical to develop a method for the mass production of VACNT arrays.

\* Corresponding author. Fax: +86 10 6277 2051.

E-mail address: [wf-dce@tsinghua.edu.cn](mailto:wf-dce@tsinghua.edu.cn) (F. Wei).

<sup>1</sup> Current address: Department of Chemical Engineering, Case Western Reserve University, Cleveland, OH 44106, USA. 0008-6223/\$ - see front matter © 2009 Elsevier Ltd. All rights reserved.

doi:10.1016/j.carbon.2009.11.043

Chemical vapor deposition (CVD) is the most powerful way for controllable growth of CNTs. One of the most popular ways for the mass production of CNTs is fluidized bed catalytic chemical vapor deposition (CVD) [24–26]. The fluidized bed reactor has great advantages in terms of providing enough space for CNT growth, excellent diffusion and heat transfer, easy scaling up and continuous operation, and so on. A pilot mass production of agglomerated multi-walled CNTs (MWCNTs) with high yield (15 kg/h) was realized in a fluidized bed reactor in 2002 [27]. Up to now, agglomerated single/double/few-walled CNTs can also be mass produced in a fluidized bed reactor. The researches on the production of CNTs have been reported by many groups, including Wei [26–29], Serp [24,30–32], Windle [33], See and Harris [25,34,35], Hee [36], Xu and Zhu [37], Rakov [38], Yang [39], Heish [40,41], and others. The products of the fluidized bed process mentioned above were agglomerated CNTs. While for VACNT arrays, they were commonly synthesized on a flat substrate using various CVD methods in a fixed bed [14,18–22]. However, the flat substrates always possess low specific surface area ( $<0.5 \text{ m}^2/\text{g}$ ), which limits the mass production of VACNT arrays. Besides, it is difficult to suspend or move the flat substrate by gas flow or other methods because of the anisotropic morphology of a flat substrate, which results in its poor mobility. Thus, the yield of VACNT arrays grown on a flat substrate is very limited. Later, various particles with larger surface area, such as spheres [23,42,43], fibers [44], flakes [45], were used for the growth of VACNT arrays in large quantities. Recently, a strategy for VACNT arrays grown among lamellar catalyst was developed [46]. Compared with flat substrate (about  $4 \text{ cm}^2/\text{g}$  for wafer with a thickness of 0.1 mm) or spherical substrate (about  $400 \text{ cm}^2/\text{g}$  for spheres with a diameter of 0.7 mm) with limited surface area, the lamellar catalysts were with much larger specific surface area (higher than  $30,000 \text{ cm}^2/\text{g}$ ), providing enough surface area for the growth of VACNT arrays. Meanwhile, the size of the lamellar catalysts can be limited into A particles according to Geldart particles classification to simplify the operation in the fluidized bed. It shows a potential way for the mass production of VACNT arrays in a fluidized bed reactor [47]. However, the effects of various key parameters on the growth behavior of CNT arrays intercalatedly grown on lamellar compounds were still unclear.

Herein, a fluidized bed CVD process was comprehensively developed for the mass production of VACNT arrays intercalatedly grown among vermiculites. Various key parameters were investigated, including the catalyst loading amount, catalyst reduction time, growth temperature, space velocity, and apparent gas velocity. Based on the parameter study, VACNT arrays with a yield of 3.0 kg/h were produced under optimized conditions in a pilot plant fluidized bed reactor.

## 2. Experimental

Vermiculite, a clay mineral which is a group of micaceous hydrated silicate minerals related to the chlorites and used in heat-expanded form as insulation and as a planting medium, was used as carrier of the catalyst. The vermiculite used in our experiment was mined in Lingshou, Hebei Province of

China. In brief, vermiculite powder with a size of 100–250  $\mu\text{m}$  (bulk density of about  $160 \text{ kg}/\text{m}^3$ ) was suspended in distilled water to form a uniform suspension through strong stirring at 80 °C. Subsequently, a solution of iron nitrate ( $\text{Fe}(\text{NO}_3)_3 \cdot 9\text{H}_2\text{O}$ ) and  $(\text{NH}_4)_6\text{Mo}_7\text{O}_{24} \cdot 4\text{H}_2\text{O}$  was mixed with the suspension quickly. The obtained mixture was kept at 80 °C for 5 h. After filtration, the filtrated cake was dried at 110 °C for 12 h and further calcined at 400 °C for 1 h. Then the lamellar Fe/Mo/vermiculite catalyst for the production of VACNT arrays was obtained.

The schematic diagram of the apparatus used in the experiment is similar to the previous studies [47]. Here, the lamellar Fe/Mo/vermiculite was used as catalyst. About 5.0 g catalyst was fed into the reactor before reaction. The quartz fluidized bed reactor was then heated to reaction temperature in argon atmosphere. After reduction by  $\text{H}_2$ , a mixture of carbon source/ $\text{H}_2$  was introduced into the fluidized bed and the reaction occurred within the vermiculite particles. The catalysts were smoothly fluidized in the reactor. After the reaction, the fluidized bed reactor was cooled under argon atmosphere. The carbon product was collected and characterized as follows.

The morphology of the VACNT arrays was characterized using scanning electron microscope (SEM, JSM 7401F). Transmission electron microscopy (TEM) studies were performed on a JEOL JEM 2100 TEM with an accelerating voltage of 120 kV. For TEM analysis, a dilute suspension of VACNT arrays was prepared in ethanol using ultra-sonication technique and then 0.5 ml solution was dropped onto a Lacey carbon coated Cu grid. Raman experiments were also performed on a Renishaw RM2000 Raman spectrophotometer, at room temperature, using a linearly polarized He–Ne laser ( $\lambda = 632.8 \text{ nm}$ ). The diameter of the laser spot was 3–5  $\mu\text{m}$  and the resolution of the spectrometer was about  $1 \text{ cm}^{-1}$ . The purity of CNTs in the as-grown product was obtained from thermogravimetry analysis (TGA) by a TGA Q500. Samples were positioned in a platinum pan in an atmosphere of air flowing at 20 mL/min and analyzed with a heating rate of 20 °C/min up to 900 °C. Tests of  $\text{H}_2$ -TPR of the Fe/Mo/vermiculite catalyst were conducted using a fixed-bed continuous-flow microreactor or adsorption–desorption system. A KOH column and a 3A zeolite molecular sieve column were installed in sequence at the reactor exit to remove water vapor formed by the reduction of metallic oxide components of the catalyst sample. The ramp rate of temperature was 10 °C/min. Change of  $\text{H}_2$  signal was monitored using on-line GC (Shimadzu GC-8A) with a TC detector. 50 mg of Fe/Mo/vermiculite catalyst sample was first flushed by an Ar (of 99.999% purity, 20 sccm/min) stream at 673 K for 60 min to clean the surface, and then cooled down to room temperature, followed by switching to a  $\text{N}_2$ -carried 5.24 vol.%  $\text{H}_2$  gaseous mixture (20 sccm/min) as reducing gas to start the TPR observation.

## 3. Results and discussion

Natural vermiculites with a size of 100–250  $\mu\text{m}$ , were selected as the substrate for CNT arrays. As reported in the previous report [47], they are easily to be fluidized with a gas velocity ranging from 7 to 24 cm/s. After the impregnation and drying,

the active phase can be intercalated among the catalyst layers. The specific surface area of the vermiculite substrate used is about  $4.5 \text{ m}^2/\text{g}$ . In order to evaluate the performance of the lamellar Fe/Mo/vermiculite catalyst on the growth of VACNT array, various key parameters including the loading amount of active phase, growth temperature, reduction, space velocity, and apparent gas velocity in the fluidized bed, were investigated. The details can be found as follows.

### 3.1. Effect of loading amount of active phase among lamellar substrate

Through the ion exchange process, the metal catalysts were intercalated among the vermiculites with the mass ratio of Fe to vermiculite ranging from 0.0075 to 0.300, which were

named as catalyst A–F as shown in Table 1. After a 30-min growth, the morphology of the as-grown products on catalyst A–F is shown in Fig. 1. Unlike agglomerated CNTs grown on powder catalyst [24–26,30–34,36–41], CNTs with good alignment were synchronously grown among the layers in this situation. The synthesized CNTs were vertically aligned on the lamellar substrate and the length of the arrays was about several micrometers. However, the fine structure of the arrays grown on catalyst A–F was different. As shown in Fig. 1a, the CNTs in array form grown on catalyst A were with uniform length of about  $8.8 \mu\text{m}$ . When the loading amount increased to 0.01875 (Catalyst B), the yield of CNT arrays increased from 0.355 to  $1.167 \text{ g}_{\text{CNT}}/\text{g}_{\text{cat}}$  (Table 1), which was mainly attributed to the increasing density of active catalyst particles. However, the length of CNT decreased to  $3.8 \mu\text{m}$

**Table 1 – The carbon yields and  $I_D/I_G$  value of Raman spectra for VACNT arrays intercalatedly grown at  $650 \text{ }^\circ\text{C}$  for 30 min on Fe/Mo/vermiculite catalysts.**

Catalyst	$m_{\text{Fe}}/m_{\text{vermiculite}}^{\text{a}}$	$m_{\text{Mo}}/m_{\text{vermiculite}}^{\text{a}}$	Carbon yield ( $\text{g}_{\text{CNT}}/\text{g}_{\text{cat}}$ ) <sup>b</sup>	$I_D/I_G$ ratio <sup>c</sup>
A	0.0075	0.0025	0.355	1.03
B	0.01875	0.0038	1.167	1.01
C	0.0375	0.0094	1.118	1.00
D	0.075	0.0125	0.845	0.88
E	0.150	0.030	0.628	1.35
F	0.300	0.060	0.224	1.20

a The amount of Fe and Mo was that intercalated among the vermiculite layers.

b The carbon yields were measured by TGA.

c The  $I_D/I_G$  ratio was obtained from the Raman spectra.

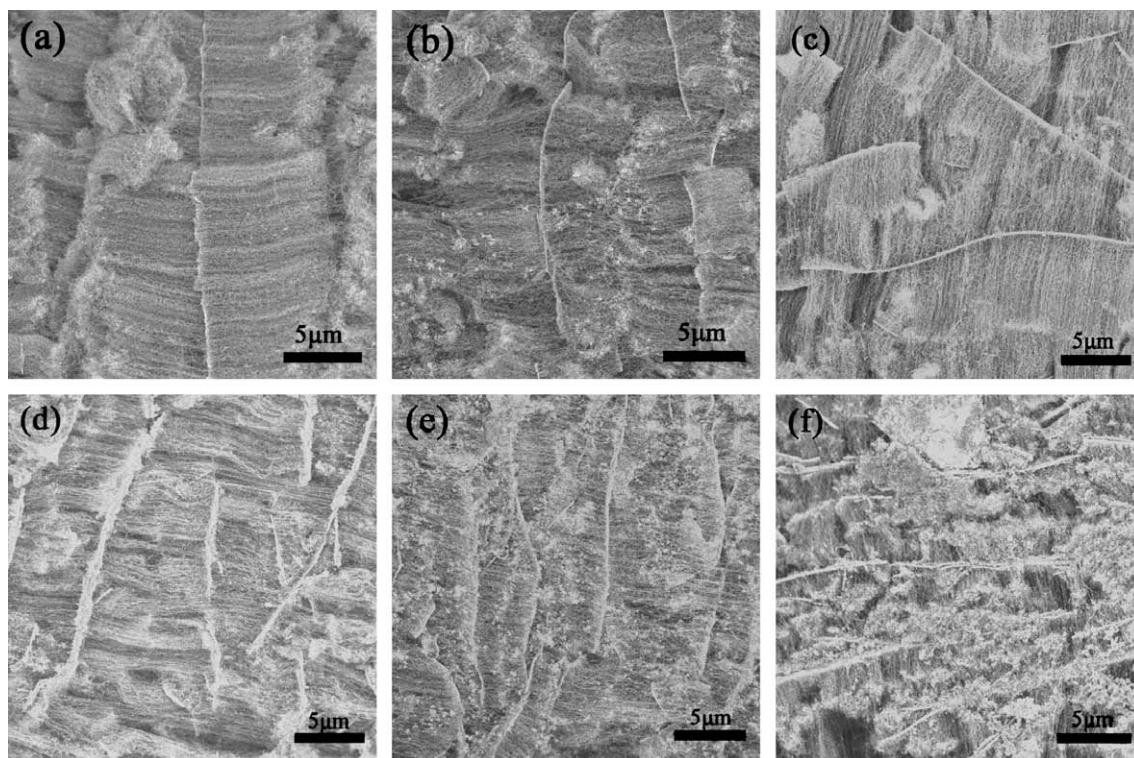


**Fig. 1 – The morphology of the VACNT arrays among Fe/Mo/vermiculite catalyst layers with different loading amount at  $650 \text{ }^\circ\text{C}$  for 30 min. The mass ratios of Fe to vermiculite are (a) 0.0075, (b) 0.0188, (c) 0.0375, (d) 0.0750, (e) 0.150, and (f) 0.300.**

(Fig. 1b). With further increased loading amount, more active sites formed among the layers of vermiculite, leading to the formation of more CNTs among the vermiculite layers. However, the stress between vermiculite layers and CNT arrays increased obviously due to the increasing mismatch among CNTs and the vermiculite crushed into small pieces, accordingly. The VACNT arrays intercalated among disordered vermiculite layers, with non-uniform length (Fig. 1c–f). While under high Fe loading amount, some of the catalyst particles

decorated on the exterior surface of vermiculite, which caused the formation of random CNTs on the exterior surface of the lamellar substrate. It was noticed from Fig. 1b–f that with higher Fe loading amount, both the lengths and the yields of VACNT arrays among lamellar catalyst decreased significantly (Table 1), which can be attributed to the strong stress that limited the further growth of VACNT arrays. Meanwhile, the ratios of D peak to G peak were larger with higher loading amount when the mass ratio of Fe ranged from 0.075

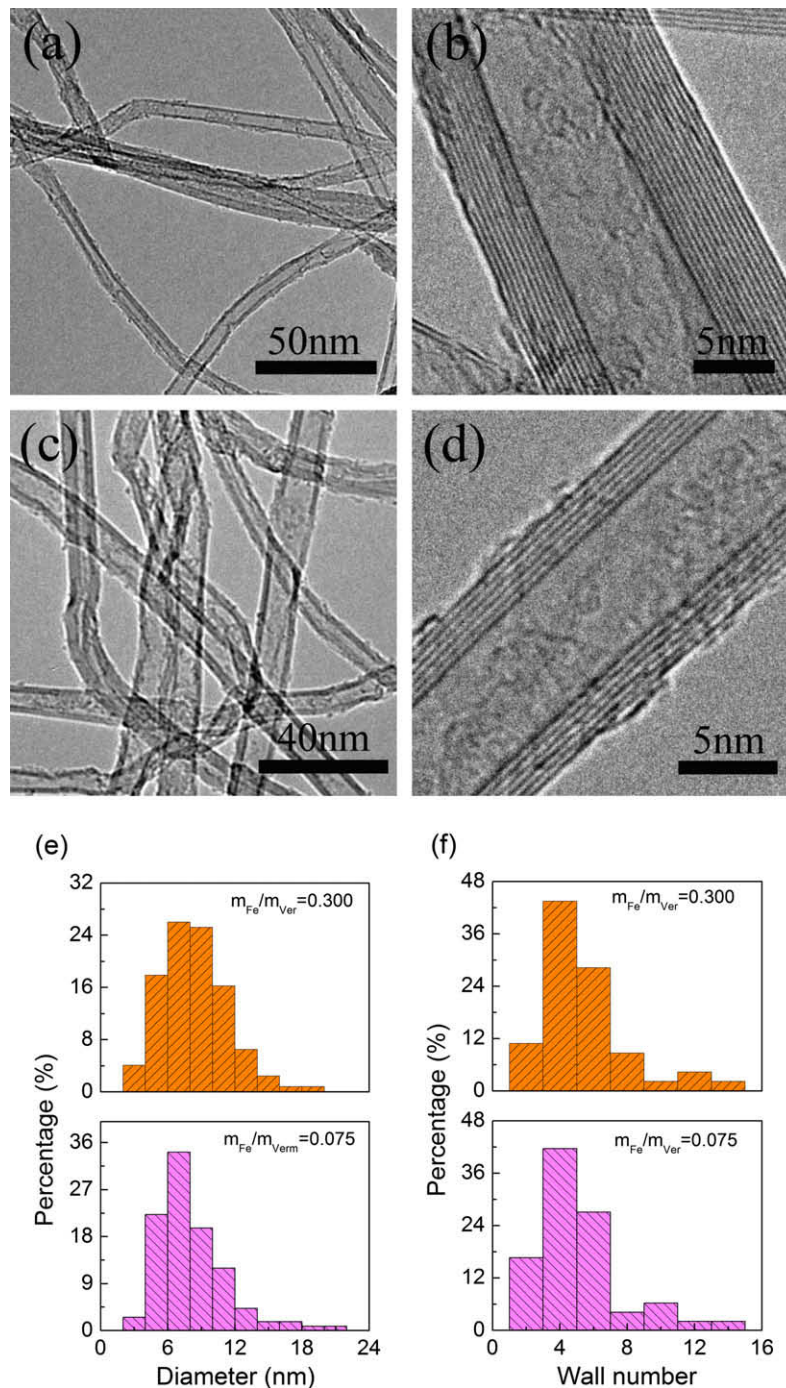


**Fig. 2** – TEM and high resolution TEM of VACNT arrays grown among vermiculite layers at 650 °C on (a) and (b) catalyst A and (c) and (d) catalyst F, respectively. The diameter and wall number distributions of as-grown CNTs in the arrays grown on catalyst A and catalyst F were illustrated in (e) and (f), respectively.

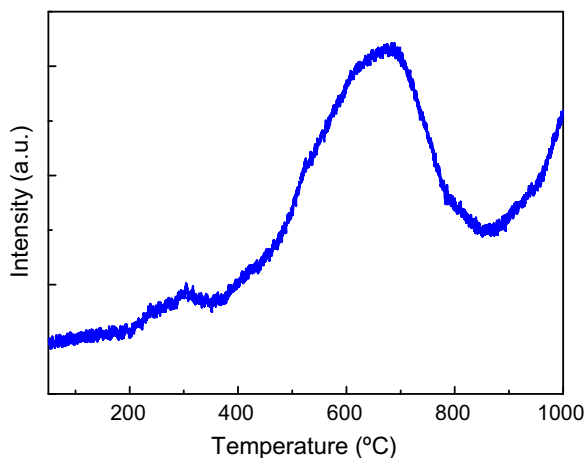


**Fig. 3** – The TPR pattern of the Fe/Mo/vermiculite catalyst C.

to 0.300 (as shown in Table 1), indicating the existence of more defects. To characterize the diameter distribution of CNTs intercalated among the lamellar catalyst, TEM images were taken as shown in Fig. 2. It could be found that the main products were CNTs (Fig. 2a–d), the inner diameter of which was 3–7 nm, while the outer diameter was approximately 6–20 nm (Fig. 2e). The ratio of wall thickness to the diameter was about 50% and the wall number ranged mainly from 3 to 10 (Fig. 2f). The diameter slightly increased with higher loading amount because of the formation of larger Fe parti-

cles, which was similar to many reports [48–51]. To get high yield of VACNT arrays with high quality, catalyst C with optimized loading amount (a mass ratio of Fe to vermiculite of 0.0375) was used for further parameter tests.

### 3.2. Effect of $H_2$ reduction

The first step for the intercalated growth of VACNT arrays on lamellar catalyst was the reduction of  $Fe_xO_y$  into Fe particles during CVD process. The  $H_2$ -TPR spectra of catalysts C is shown in Fig. 3. There is a main reduction peak starting from 500 °C, and ended at 800 °C, indicating that most Fe atoms exist in Fe/Mo alloy form [52–54]. It should be noticed that there are another two reduction peaks at 330, 470 °C, which can be assigned to the reduction of  $Fe_2O_3$  to  $Fe_3O_4$ ,  $Fe_3O_4$  to FeO, respectively [53,55]. The reduction of FeO to Fe occurs at about 600 °C, which is coincided with the reduction of Fe/Mo alloy. It indicates that in Catalyst C, the initial Fe will mainly form Fe/Mo alloy phase, while a small part of Fe will be in the form of  $Fe_2O_3$ . After the reduction with a temperature higher than 550 °C, Fe catalyst particles formed among the vermiculite layers. Furthermore, the effect of initial  $H_2$  reduction at 650 °C is tested with different amount of hydrogen introduced into the reactor. When no  $H_2$  was introduced into the reactor, no VACNT arrays can be synthesized, as shown in Fig. 4a. With longer reduction time, namely more introduced  $H_2$ , the length of the as-grown VACNT arrays increased (Fig. 4b–d), indicating the increasing activity for VACNT array growth.

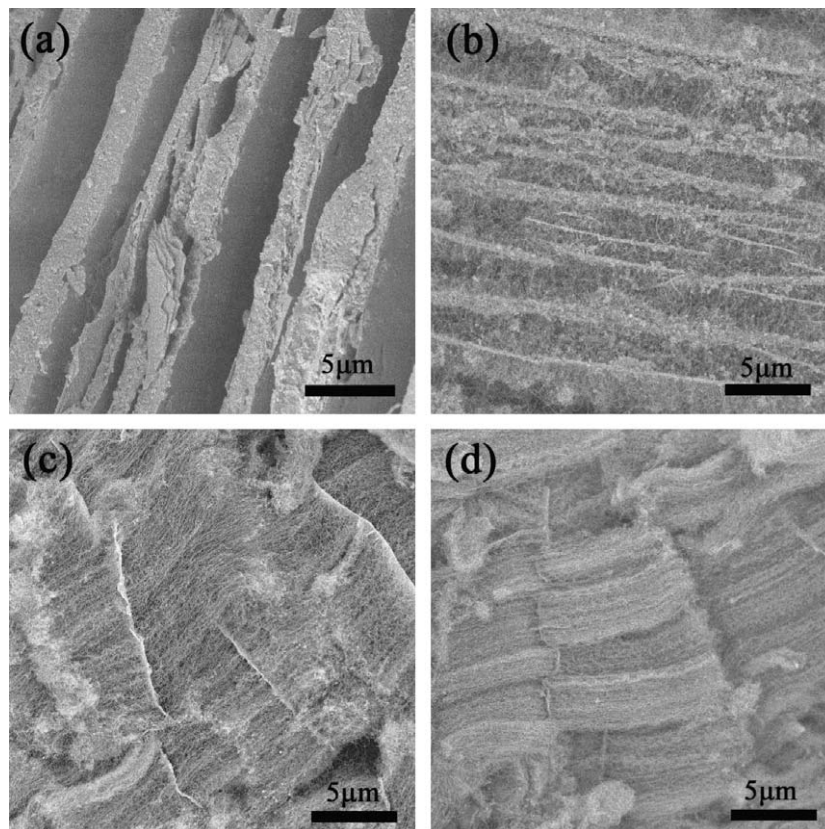


**Fig. 4** – The morphology of the VACNT arrays grown among Fe/Mo/vermiculite layers at 650 °C for 30 min with reduction time of (a) 0 min, (b) 1 min, (c) 10 min and (d) 30 min.

The length of VACNT arrays reached 10  $\mu\text{m}$  when the reduction time increased to 30 min. Furthermore, the yield (Fig. 5a) and the ratio of D peak to G peak (Fig. 5b) of VACNT arrays changed from 1.35 to 0.77, respectively. With more  $\text{H}_2$  introduced to the reduction process, the density of reduced Fe particles and activity of catalyst particles increased. Thus, the CNTs grew synchronously and formed longer VACNT arrays [56]. The yield of VACNT arrays became larger. Meanwhile, when the ratio of  $\text{H}_2$  to  $\text{Fe}_2\text{O}_3$  increased, the activity of Fe catalyst increased. The CNTs grew continuously and

the defect density decreased (Fig. 5b). Moreover, if the CNTs were synthesized in  $\text{H}_2$  atmosphere, the sintering of metal catalyst on the surface of lamellar catalyst became serious [29], leading to the formation of CNTs with larger diameter.

### 3.3. Effect of growth temperature

After reduction, the growth of VACNT arrays was carried out at various growth temperatures (Figs. 6–8). To determine a good domain for the growth of VACNT arrays, the effect of

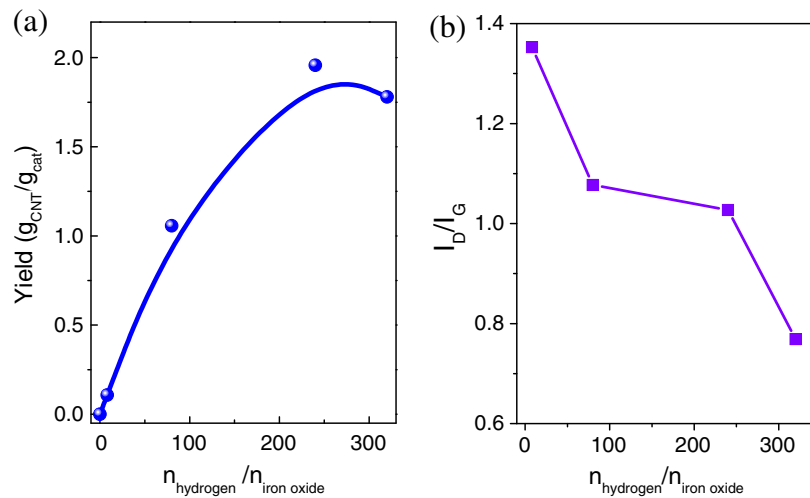


Fig. 5 – (a) The yield and (b) intensity ratio of D peak to G peak of VACNT arrays grown among Fe/Mo/vermiculite layers at 650 °C for 30 min with different reduction times.

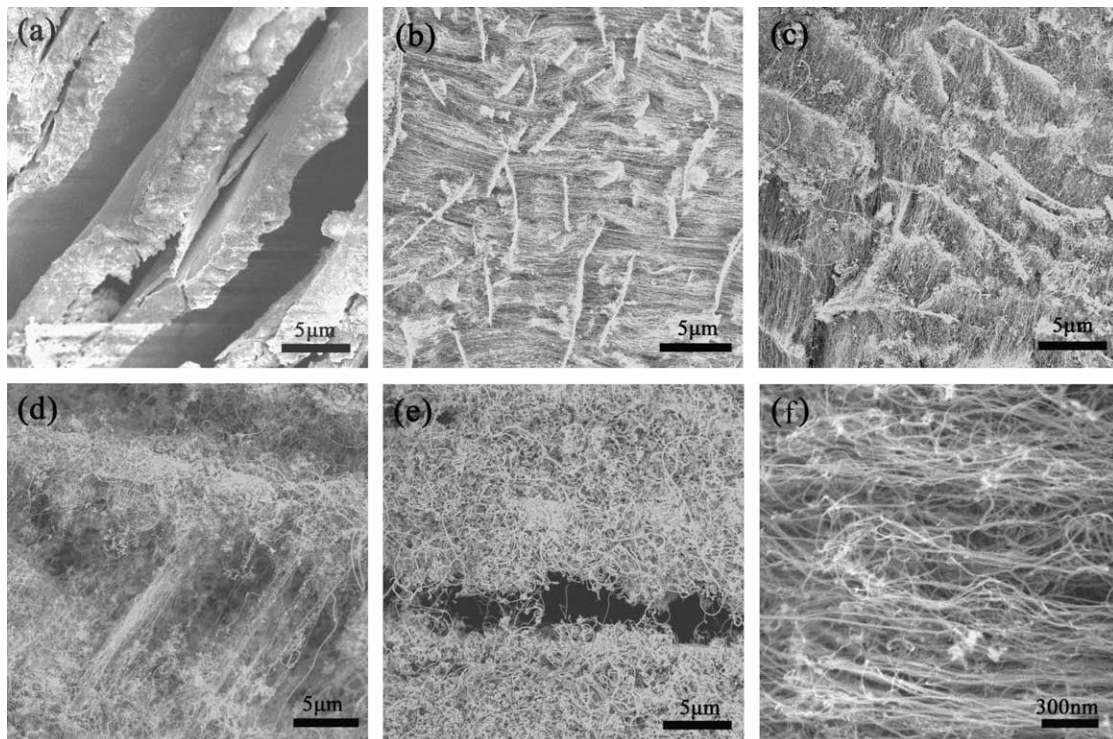


Fig. 6 – The morphologies of the CNTs grown among Fe/Mo/vermiculite catalyst layers for 30 min at (a) 550 °C, (b) 650 °C, (c) 750 °C, (d) 850 °C, (e) 950 °C. (f) High magnification SEM image of CNTs grown at 650 °C.

growth temperature was investigated. The catalyst was reduced at growth temperature for 30 min at first, and then  $C_2H_4$  was introduced. The as-grown products were shown in Fig. 6. At 550 °C, nearly no VACNT arrays were synthesized due to the low density of active Fe catalyst particles and low  $C_2H_4$  cracking rate (Fig. 6a). When the temperature increased to 650 °C, CNTs with good alignment intercalatedly grew among vermiculites and the length of the VACNT arrays was 2–4  $\mu\text{m}$  (Fig. 6b and f). The alignment of CNTs became disordered. Some CNTs entangled with each other when it grew at 750 °C (Fig. 6c). However, the main products were still short

VACNT arrays (Fig. 6c). If the growth temperature further increased, the ratio of arrays in the as-grown products decreased. As demonstrated in Fig. 6d, few aligned CNT bundles were observed, while most CNTs were randomly agglomerated around the lamellar layers. Agglomerated CNTs with high densities are shown in Fig. 6e (grown at 950 °C), and few CNTs in array form could be found. The alignment of CNTs intercalatedly grown among the lamellar catalysts became worse with increasing growth temperature. Thus, the growth temperature influenced the morphology of the CNTs significantly.

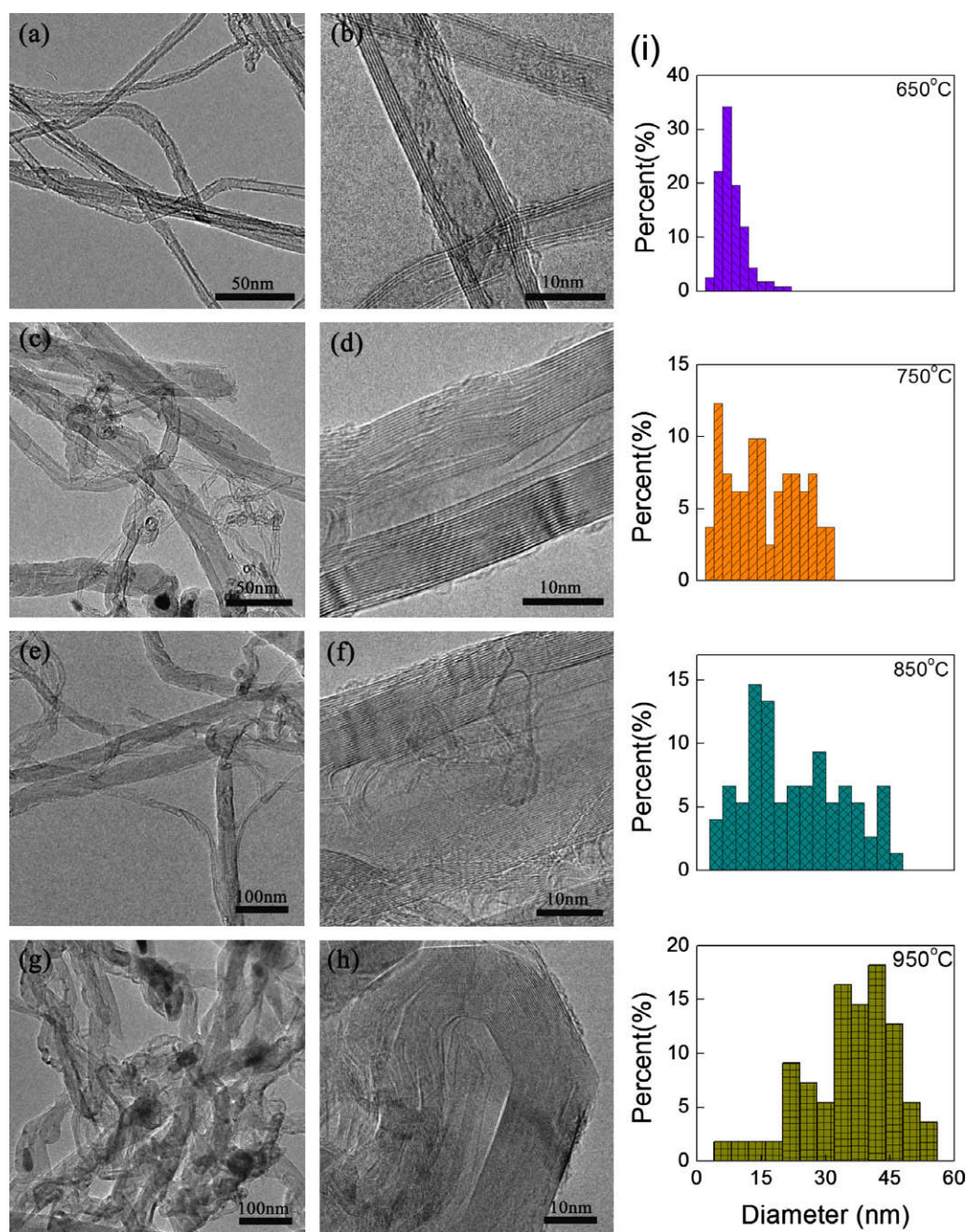


Fig. 7 – The TEM images of the CNTs grown among Fe/Mo/vermiculite layers for 30 min at (a) and (b) 650 °C, (c) and (d) 750 °C, (e) and (f) 850 °C, (g) and (h) 950 °C; (i) The diameter distributions of CNTs among Fe/Mo/vermiculite layers at different growth temperature.

Meanwhile, the diameter distributions of CNTs in the arrays were further investigated by TEM. As illustrated in Fig. 7, thin wall CNTs with diameter ranging from 4 to 10 nm were obtained in the products grown at 650 °C (Fig. 7a, b, i). The wall numbers were mainly 4–7. The ratio of wall thickness to diameter was about 0.5. If the growth

temperature increased to 750 °C, the diameter of as-obtained CNTs increased obviously. The TEM images (Fig. 7c, d, i) showed the thin wall CNTs with a diameter of 10 nm and thick wall CNTs with a diameter of 30 nm. Besides, it can be observed from the high resolution TEM images (as shown in Fig. 7d) that the inner wall of the CNTs became discontinuous.

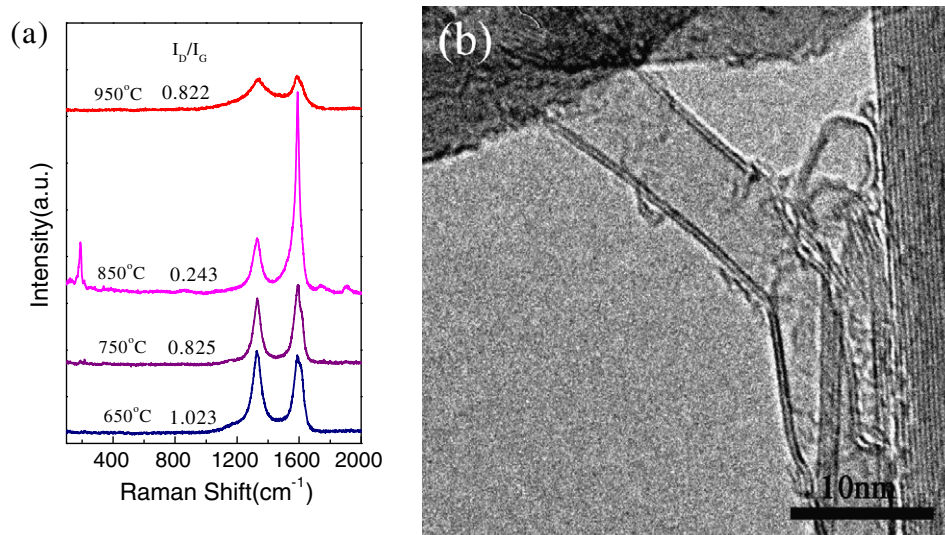


Fig. 8 – (a) The Raman spectra of as-grown CNTs among Fe/Mo/vermiculite layers at different growth temperature. (b) High resolution TEM image of thin wall CNTs in the as-grown products of VACNT arrays grown at 850 °C.

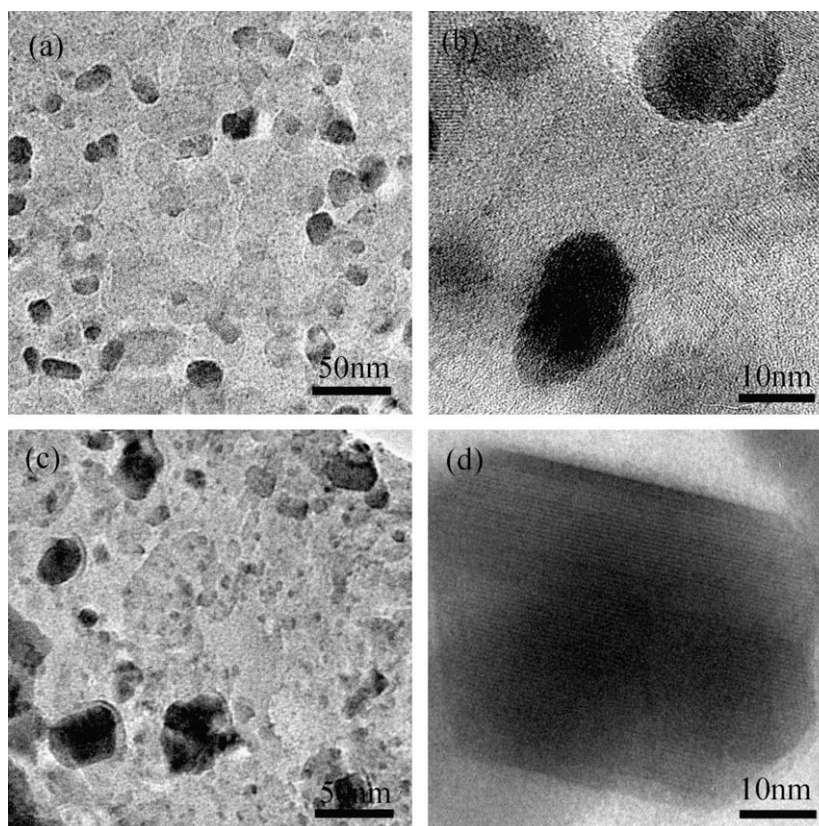


Fig. 9 – TEM and high resolution TEM images of catalyst A reduced at (a) and (b) 650 °C and (c) and (d) 950 °C, respectively.

The CNTs of large diameter were with more defects. If the temperature further increased, the sintering among the catalyst became more severe, leading to the formation of more CNTs with larger diameter at the growth temperature of 850 °C (Fig. 7e, f, i). However, there were still some double-walled CNTs (DWCNTs) (Fig. 8), which will be mentioned later. If the growth temperature increased to 950 °C, as illustrated in

Fig. 7g, h, i, the as-grown CNT products with higher defect densities showed large diameter of around 45 nm. The Raman spectra as shown in Fig. 8 were also employed to characterize the quality of the as-obtained CNTs. Typical D peak and G peak were shown for products grown at various reaction temperatures (Fig. 8a). For the CNT products grown at 850 °C, a radial breathing mode peak at 191  $\text{cm}^{-1}$  was observed in Fig. 8a,

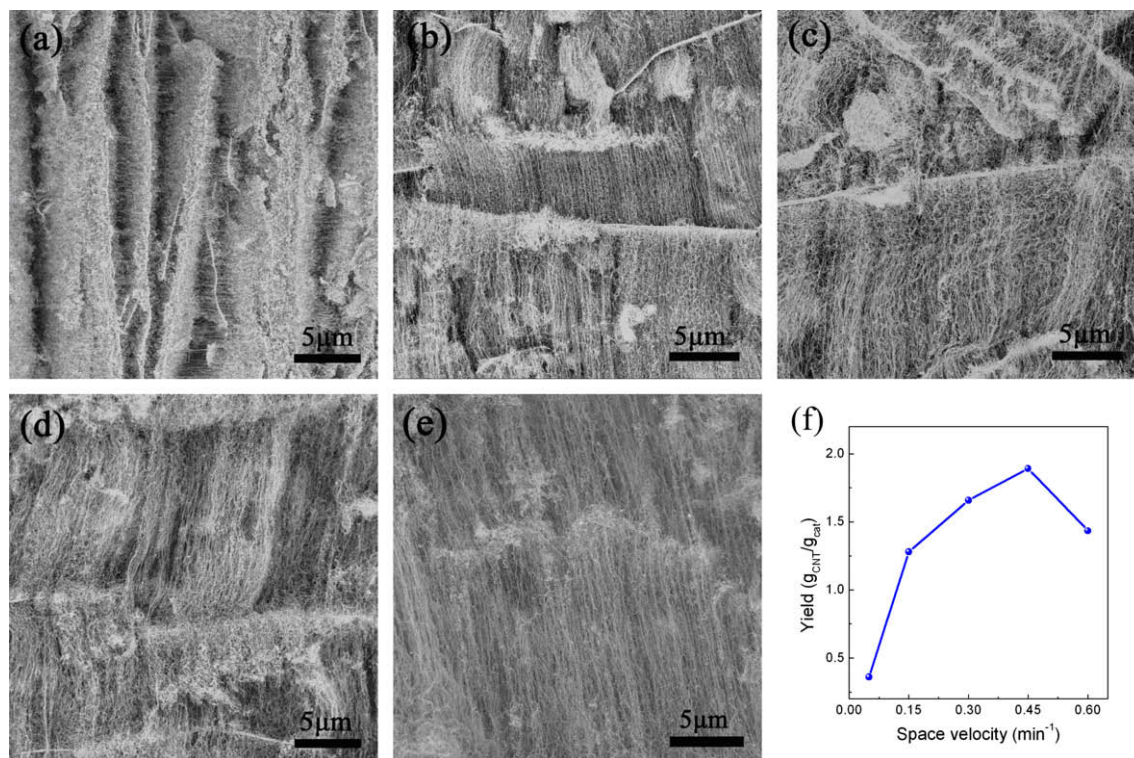


Fig. 10 – The morphologies of VACNT arrays among vermiculite substrate with different space velocities: (a)  $0.05 \text{ min}^{-1}$ , (b)  $0.15 \text{ min}^{-1}$ , (c)  $0.30 \text{ min}^{-1}$ , (d)  $0.45 \text{ min}^{-1}$ , (e)  $0.60 \text{ min}^{-1}$ . (f) The yields of VACNT arrays among vermiculite substrate at different space velocities.

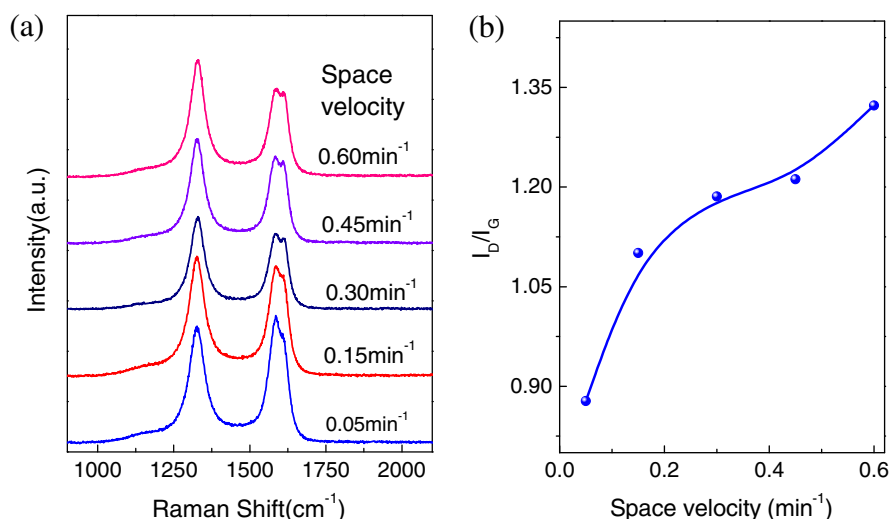
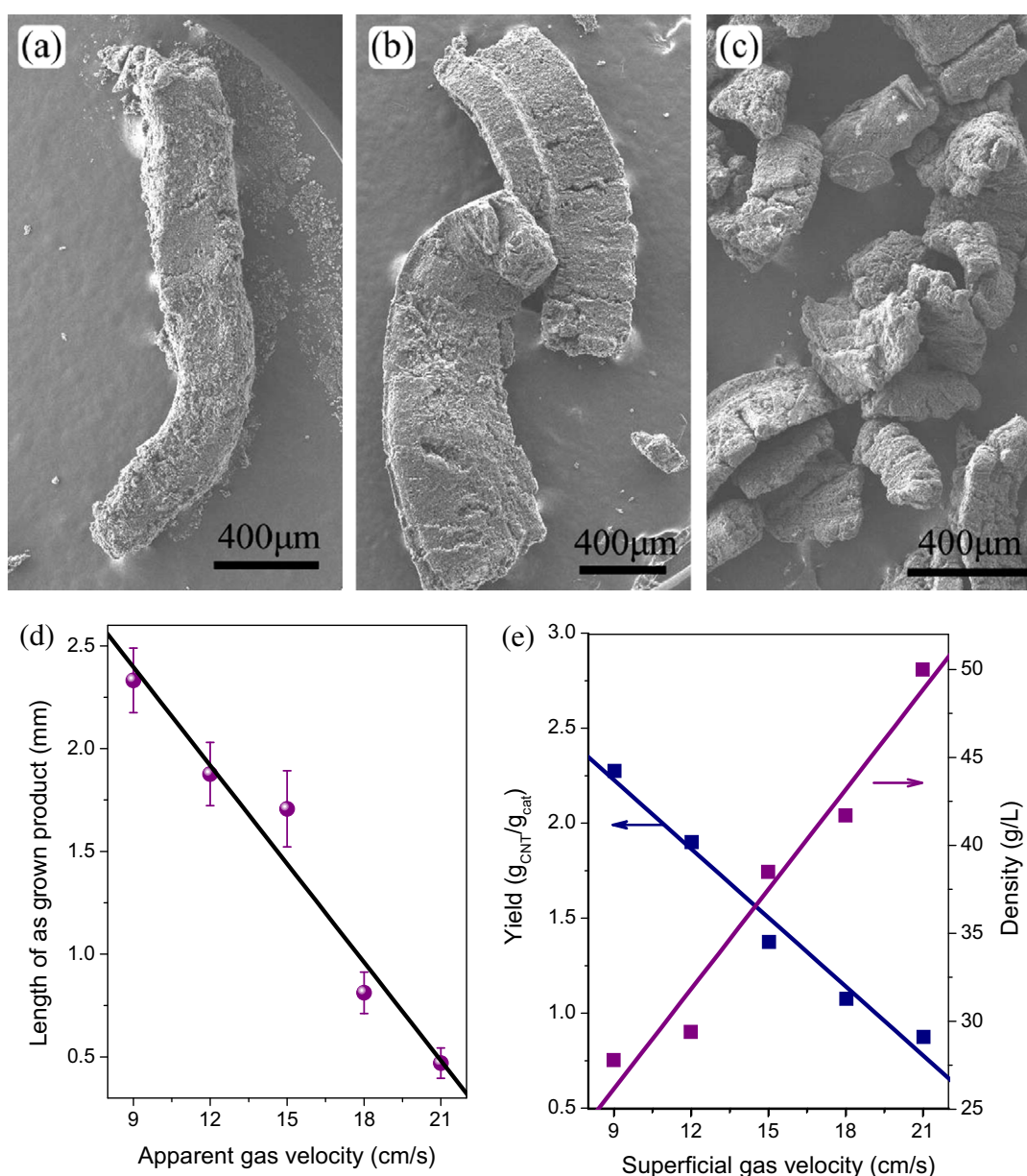


Fig. 11 – (a) The Raman spectra and (b)  $I_D/I_G$  ratio of VACNT arrays among vermiculites layers under different space velocities of  $\text{C}_2\text{H}_4$ .

indicating the existence of few-walled CNTs with small diameter. From the high resolution TEM image shown in Fig. 8b, some DWCNTs were found in the as-grown product. It is commonly believed that MgO is one of the major compositions of the vermiculite catalyst, and Fe/Mo/MgO is very active for the growth of DWCNTs at high temperature [28,57–60]. The existence of DWCNTs in the products caused the significant increase of the Raman signals and the intensity of G band.

The dependence of the CNTs on growth temperature was mainly related to the change on size distribution of catalyst particles and their growth behavior. Under different reduction/growth temperature, the catalyst particles showed quite different morphology, as indicated by Fig. 9. For example, when the reduction/growth temperature was 650 °C, Fe parti-

cles were with a uniform size of 10–20 nm, and a density of  $8.5 \times 10^{14} \text{ m}^{-2}$  among the vermiculite layers (Fig. 9a and b). Thus, CNTs grew at a similar rate in high density. They were self-organized into the aligned morphology, and VACNT arrays were intercalatedly grown among vermiculite catalysts [56]. If the reduction/growth temperature increased to 950 °C, Fe catalyst particles were with a bimodal size distribution of 1–5, 40–60 nm, respectively (Fig. 9c). The small catalyst particles were mainly reduced from the Fe/Mo alloy at high temperature (Fig. 3), and they were efficient for the growth of few-walled CNTs (Fig. 7i). While the large Fe catalyst particles were speculated to be the result of sintering from the pre-reduced Fe catalyst at low temperatures (Fig. 3). They were of good crystallization (Fig. 9d), and effective for the growth of



**Fig. 12** – The morphology of VACNT arrays among vermiculites with different superficial gas velocities: (a) 9.0 cm/s, (b) 15.0 cm/s, (c) 21.0 cm/s. (d) The size of as-grown intercalated VACNTs with different superficial gas velocities. (e) The VACNT yield and densities of products grown at different superficial gas velocities.

CNTs with large diameter. However, it should be noticed that the growth rate of few-walled CNTs was very fast, while the growth rate of large diameter CNTs was relatively low [20,21,29]. The few-walled CNTs were prone to grow among porous catalyst, and the metal catalysts lose activity quickly [61]. Furthermore, it should be noticed that the amount of alkali metal (naturally existed in vermiculites) assisted the sintering of Fe catalyst particles and absorbed on their surface at high temperature. The volume diffusion of carbon atoms through catalyst particles was strongly affected by the alkali metals. Because of the migration of alkali ions on the surface, the precipitation of carbon atoms became unstable and the CNT growth became discontinuous, leading to the slow growth rate of CNTs and high defect density [62] (Fig. 8a), especially the inner cone of CNTs with large diameter. The large growth rate difference and fast deactivation of Fe catalyst caused the random agglomeration growth behavior of CNTs, and the formation of entangled CNTs consequently (Fig. 6e) [63]. Those results indicated that both the structure and agglomeration behavior of the as-grown CNTs were sensitive to the growth temperature.

### 3.4. Effect of space velocity

The space velocity is the mass ratio of introduced carbon source to the catalyst in fluidized bed. It is widely accepted to characterize the activity of catalyst in heterogeneous reaction, which is also a key parameter for scaling up. Here, the influence of different space velocities on the growth behavior of CNTs was investigated. The as-grown products at different space velocities were shown in Fig. 10. With increasing the space velocity, more  $C_2H_4$  was introduced into the reactor, and the concentration increased as well. The concentration gradient between the main phase and lamellar substrate became larger, indicating more  $C_2H_4$  can diffuse into the active sites. Thus, the length of arrays intercalated among the vermiculites increased gradually (Fig. 10a–e). Furthermore, the yields of the VACNT arrays also increased significantly with the increasing space velocity (Fig. 10f). When the space velocity reached  $0.60 \text{ min}^{-1}$ , the CNT density decreased which was assumed to be caused by the fast deactivation of catalyst particles. Raman spectra of the as-grown products on catalyst C are shown in Fig. 11a. The  $I_D/I_G$  ratio increased gradually with the increment of the space velocity (Fig. 11b). Thus it is concluded that CNTs grown at higher space velocity are with more defects.

### 3.5. Effect of apparent gas velocity

The apparent gas velocity determines the fluidized state of particles in the fluidized bed reactor. From the fluidization curves shown in the previous studies [47], it can be seen that if the gas velocity is in the scope of 9.0–21.0 cm/s, the catalysts behave like a fluid. In this status, the catalysts tend to establish a level and flows in response to pressure gradients, which is mainly identified as particulate fluidization. With the increasing gas velocity, the flow patterns or regimes turn into bubbling fluidization, and turbulent fluidization. Here, the collision among particles increased with the increasing gas velocity, and the size of as-grown products reduced signif-

icantly. When the apparent gas velocity was 9.0 cm/s, the as-grown products showed a worm-like structure with a length of 2.4 mm (Fig. 12a). If the apparent gas velocity further increased, the collisions among particles became more frequent and violent in the bubbling fluidization and turbulent fluidization. Thus, the particle size decreased and the products showed spherical morphology (Fig. 12a–d). Meanwhile, the carbon yields decreased and the densities of as-grown products increased (Fig. 12e). That was attributed to fewer CNTs grown among vermiculites at high gas velocity and short residue time.

### 3.6. Scale up of fluidized bed in a pilot plant fluidized bed reactor

Generally, for a new chemical process, a pilot plant at the productivity of 20–300 tons/year is necessary, although it is difficult for its large amount of research work and is uneconomical due to its small productivity. Base on the above understanding and optimization, a pilot plant fluidized bed reactor with a diameter of 500 mm was used for mass production of VACNT arrays (Fig. 13). The VACNT arrays can be successful produced in the fluidized bed with a productivity of 3.0 kg/h (24 tons/year). This is equivalent to the productivity of  $10^8$  spheres [23,42] or about  $1.5 \times 10^5$  1 in. wafers [14,18,19] as substrate using  $C_2H_4$  as carbon source (assuming that the density of the VACNT arrays on wafer is 40 g/L and the length is 3.0 mm for 1 h growth). This is the first mass production route of simultaneously assemble thousands of CNT arrays in a single block of natural compound [64], and a hierarchical, three-dimensional compounds with alternate CNT array and inorganic layers was available in kilogram scale.



Fig. 13 – The pilot plant facility for VACNT array production at a rate of 3.0 kg/h.

Furthermore, the as-obtained VACNT arrays can be easily purified by impregnation in 1.0 mol/L HCl solution for 1.0 h, and 1.0 mol/L HF solution subsequently. Various strategies for CNT purification can be easily found [65]. The as-obtained VACNT arrays can be sheared into fluffy CNTs and individual CNTs for further application on composites, transparent conductive film, supercapacitors, fuel cells, lithium ion secondary batteries, energy absorbing, and so on.

#### 4. Conclusions

Lamellar Fe/Mo/vermiculites with a diameter of 100–250  $\mu\text{m}$  were used as catalyst carriers for the scaled production of VACNTs. Various parameters, including catalyst loading amount, catalyst reduction conditions, growth temperature, space velocity, and apparent gas velocity were investigated to develop the process for the mass production of VACNT arrays. The main conclusions that can be drawn from the present work are:

1. The temperature influences significantly the structure of the CNTs as well as the agglomerated properties of the CNTs. The effect of the other parameters on CNTs morphology is less pronounced.
2. The reduction of catalyst is necessary and the space velocity should be kept at a medium value to attain high conversion of carbon sources.
3. The as-grown products are in large size in particulate fluidization and bubbling fluidization, while the size of the as-grown products decreased obviously in the turbulent fluidization state due to the violent collisions.

Based on the understanding of these various parameters, the output of 3.0 kg/h VACNT arrays were first demonstrated in a pilot plant fluidized bed reactor in this work, which provided an access to obtain large amount of CNT arrays for further applications in future.

#### Acknowledgements

The work was supported by the Natural Scientific Foundation of China (Nos. 20606020, 20736004, 20736007, 2007AA03Z346), the China National Program (No. 2006CB0N0702).

#### REFERENCES

- [1] Coleman JN, Khan U, Blau WJ, Gun'ko YK. Small but strong: a review of the mechanical properties of carbon nanotube-polymer composites. *Carbon* 2006;44(9):1624–52.
- [2] Endo M, Strano MS, Ajayan PM. Potential applications of carbon nanotubes. *Top Appl Phys* 2008;111:13–62.
- [3] Serp P, Corrias M, Kalck P. Carbon nanotubes and nanofibers in catalysis. *Appl Catal A – Gen* 2003;253(2):337–58.
- [4] Zhang J, Liu X, Blume R, Zhang AH, Schlogl R, Su DS. Surface-modified carbon nanotubes catalyze oxidative dehydrogenation of *n*-butane. *Science* 2008;322(5898):73–7.
- [5] Frank B, Zhang J, Blume R, Schlogl R, Su DS. Heteroatoms increase the selectivity in oxidative dehydrogenation reactions on nanocarbons. *Angew Chem Int Ed* 2009;48(37):6913–7.
- [6] Su DS, Chen XW, Liu X, Delgado JJ, Schlogl R, Gajovic A. Mount-etna-lava-supported nanocarbons for oxidative dehydrogenation reactions. *Adv Mater* 2008;20(19):3597–600.
- [7] Fu XB, Yu H, Peng F, Wang HJ, Qian Y. Facile preparation of RuO<sub>2</sub>/CNT catalyst by a homogenous oxidation precipitation method and its catalytic performance. *Appl Catal A – Gen* 2007;321(2):190–7.
- [8] Pan XL, Fan ZL, Chen W, Ding YJ, Luo HY, Bao XH. Enhanced ethanol production inside carbon-nanotube reactors containing catalytic particles. *Nat Mater* 2007;6(7):507–11.
- [9] Gan L, Lv RT, Du HD, Li BH, Kang FY. High loading of Pt-Ru nanocatalysts by pentagon defects introduced in a bamboo-shaped carbon nanotube support for high performance anode of direct methanol fuel cells. *Electrochem Commun* 2009;11(2):355–8.
- [10] Zou L, Lv RT, Kang FY, Gan L, Shen WC. Preparation and application of bamboo-like carbon nanotubes in lithium ion batteries. *J Power Sources* 2008;184(2):566–9.
- [11] Frackowiak E, Beguin F. Electrochemical storage of energy in carbon nanotubes and nanostructured carbons. *Carbon* 2002;40(10):1775–87.
- [12] Endo M, Kim YJ, Chino T, Shinya O, Matsuzawa Y, Suezaki H, et al. High-performance electric double-layer capacitors using mass-produced multi-walled carbon nanotubes. *Appl Phys A* 2006;82(4):559–65.
- [13] Lv RT, Kang FY, Zhu D, Zhu YQ, Gui XC, Wei JQ, et al. Enhanced field emission of open-ended, thin-walled carbon nanotubes filled with ferromagnetic nanowires. *Carbon* 2009;47(11):2709–15.
- [14] Fan SS, Chapline MG, Franklin NR, Tomblor TW, Cassell AM, Dai HJ. Self-oriented regular arrays of carbon nanotubes and their field emission properties. *Science* 1999;283(5401):512–4.
- [15] Endo M, Muramatsu H, Hayashi T, Kim YA, Terrones M, Dresselhaus NS. 'Buckypaper' from coaxial nanotubes. *Nature* 2005;433(7025):476.
- [16] Doherty EM, De S, Lyons PE, Shmeliov A, Nirmalraj PN, Scardaci V, et al. The spatial uniformity and electromechanical stability of transparent, conductive films of single walled nanotubes. *Carbon* 2009;47(10):2466–73.
- [17] Zhou CW, Kong J, Yenilmez E, Dai HJ. Modulated chemical doping of individual carbon nanotubes. *Science* 2000;290(5496):1552–5.
- [18] Li WZ, Xie SS, Qian LX, Chang BH, Zou BS, Zhou WY, et al. Large-scale synthesis of aligned carbon nanotubes. *Science* 1996;274(5293):1701–3.
- [19] Ren ZF, Huang ZP, Xu JW, Wang JH, Bush P, Siegal MP, et al. Synthesis of large arrays of well-aligned carbon nanotubes on glass. *Science* 1998;282(5391):1105–7.
- [20] Zhang XF, Cao AY, Wei BQ, Li YH, Wei JQ, Xu CL, et al. Rapid growth of well-aligned carbon nanotube arrays. *Chem Phys Lett* 2002;362(3–4):285–90.
- [21] Wei F, Zhang Q, Qian WZ, Xu GH, Xiang R, Wen Q, et al. Progress on aligned carbon nanotube arrays. *New Carbon Mater* 2007;22(3):271–82.
- [22] Singh C, Shaffer MSP, Koziol KKK, Kinloch IA, Windle AH. Towards the production of large-scale aligned carbon nanotubes. *Chem Phys Lett* 2003;372(5–6):860–5.
- [23] Xiang R, Luo G, Qian W, Wang Y, Wei F, Li Q. Large area growth of aligned CNT Arrays on spheres: towards large scale and continuous production. *Chem Vapor Depos* 2007;13(10):533–6.
- [24] Philippe R, Morançais A, Corrias M, Caussat B, Kihn Y, Kalck P, et al. Catalytic production of carbon nanotubes by fluidized-bed CVD. *Chem Vapor Depos* 2007;13(9):447–57.
- [25] See CH, Harris AT. A review of carbon nanotube synthesis via fluidized-bed chemical vapor deposition. *Ind Eng Chem Res* 2007;46(4):997–1012.

- [26] Wei F, Zhang Q, Qian WZ, Yu H, Wang Y, Luo GH, et al. The mass production of carbon nanotubes using a nano-agglomerate fluidized bed reactor: a multiscale space-time analysis. *Powder Technol* 2008;183(1):10–20.
- [27] Wang Y, Wei F, Luo GH, Yu H, Gu GS. The large-scale production of carbon nanotubes in a nano-agglomerate fluidized-bed reactor. *Chem Phys Lett* 2002;364(5–6):568–72.
- [28] Zhang Q, Yu H, Liu Y, Qian WZ, Wang Y, Luo GH, et al. Few walled carbon nanotube production in large-scale by nano-agglomerate fluidized-bed process. *Nano* 2008;3(1):45–50.
- [29] Liu Y, Qian WZ, Zhang Q, Ning GQ, Luo GH, Wang Y, et al. Synthesis of high-quality, double-walled carbon nanotubes in a fluidized bed reactor. *Chem Eng Technol* 2009;32(1):73–9.
- [30] Venegoni D, Serp P, Feurer R, Kihn Y, Vahlas C, Kalck P. Parametric study for the growth of carbon nanotubes by catalytic chemical vapor deposition in a fluidized bed reactor. *Carbon* 2002;40(10):1799–807.
- [31] Corrias M, Caussat B, Ayrat A, Durand J, Kihn Y, Kalck P, et al. Carbon nanotubes produced by fluidized bed catalytic CVD: first approach of the process. *Chem Eng Sci* 2003;58(19):4475–82.
- [32] Morançais A, Caussat B, Kihn Y, Kalck P, Plee D, Gaillard P, et al. A parametric study of the large scale production of multi-walled carbon nanotubes by fluidized bed catalytic chemical vapor deposition. *Carbon* 2007;45(3):624–35.
- [33] Li YL, Kinloch IA, Shaffer MS, Geng JF, Johnson B, Windle AH. Synthesis of single-walled carbon nanotubes by a fluidized-bed method. *Chem Phys Lett* 2004;384(1–3):98–102.
- [34] See CH, Harris AT. A comparison of carbon nanotube synthesis in fixed and fluidised bed reactors. *Chem Eng J* 2008;144(2):267–9.
- [35] See CH, Dunens OM, MacKenzie KJ, Harris AT. Process parameter interaction effects during carbon nanotube synthesis in fluidized beds. *Ind Eng Chem Res* 2008;47(20):7686–92.
- [36] Son SY, Lee Y, Won S, Lee DH, Kim SD, Sung SW. High-quality multiwalled carbon nanotubes from catalytic decomposition of carbaceous materials in gas–solid fluidized beds. *Ind Eng Chem Res* 2008;47(7):2166–75.
- [37] Xu CB, Zhu J. One-step preparation of highly dispersed metal-supported catalysts by fluidized-bed MOCVD for carbon nanotube synthesis. *Nanotechnology* 2004;15(11):1671–81.
- [38] Rakov EG, Blinov SN, Ivanov IG, Rakova EV, Digurov NG. Continuous process for obtaining carbon nanofibers. *Russ J Appl Chem* 2004;77(2):187–91.
- [39] Liu XB, Sun H, Chen Y, Lau R, Yang YH. Preparation of large particle MCM-41 and investigation on its fluidization behavior and application in single-walled carbon nanotube production in a fluidized-bed reactor. *Chem Eng J* 2008;142(3):331–6.
- [40] Hsieh CT, Lin YT, Chen WY, Wei JL. Parameter setting on growth of carbon nanotubes over transition metal/alumina catalysts in a fluidized bed reactor. *Powder Technol* 2009;192(1):16–22.
- [41] Hsieh CT, Lin YT, Lin JY, Wei JL. Synthesis of carbon nanotubes over Ni- and Co-supported CaCO<sub>3</sub> catalysts using catalytic chemical vapor deposition. *Mater Chem Phys* 2009;114(2–3):702–8.
- [42] Zhang Q, Huang JQ, Zhao MQ, Wang Y, Qian WZ, Wei F. Radial growth of vertically aligned carbon nanotube arrays from ethylene on ceramic spheres. *Carbon* 2008;46(8):1152–8.
- [43] Philippe R, Caussat B, Falqui A, Kihn Y, Kalck P, Bordere S, et al. An original growth mode of MWCNTs on alumina supported iron catalysts. *J Catal* 2009;263(2):345–58.
- [44] Zhang Q, Qian WZ, Xiang R, Yang Z, Luo GH, Wang Y, et al. In situ growth of carbon nanotubes on inorganic fibers with different surface properties. *Mater Chem Phys* 2008;107(2–3):317–21.
- [45] Pint CL, Pheasant ST, Pasquali M, Coulter KE, Schmidt HK, Hauge RH. Synthesis of high aspect-ratio carbon nanotube “flying carpets” from nanostructured flake substrates. *Nano Lett* 2008;8(7):1879–83.
- [46] Zhang Q, Zhao MQ, Liu Y, Cao AY, Qian WZ, Lu YF, et al. Energy-absorbing hybrid composites based on alternate carbon-nanotube and inorganic layers. *Adv Mater* 2009;21(28):2876–80.
- [47] Zhang Q, Zhao MQ, Huang JQ, Liu Y, Wang Y, Qian WZ, et al. Vertically aligned carbon nanotube arrays grown on a lamellar catalyst by fluidized bed catalytic chemical vapor deposition. *Carbon* 2009;47(11):2600–10.
- [48] Nasibulin AG, Pikhitsa PV, Jiang H, Kauppinen EI. Correlation between catalyst particle and single-walled carbon nanotube diameters. *Carbon* 2005;43(11):2251–7.
- [49] Harutyunyan AR, Tokune T, Mora E, Yoo JW, Epstein AJ. Evolution of catalyst particle size during carbon single walled nanotube growth and its effect on the tube characteristics. *J Appl Phys* 2006;100(4):044321-1–8.
- [50] Zhang Q, Huang JQ, Zhao MQ, Qian WZ, Wei F. Modulating the diameter of carbon nanotubes in array form via floating catalyst chemical vapor deposition. *Appl Phys A* 2009;94(4):853–60.
- [51] Celnik M, West R, Morgan N, Kraft M, Moisala A, Wen J, et al. Modelling gas-phase synthesis of single-walled carbon nanotubes on iron catalyst particles. *Carbon* 2008;46(3):422–33.
- [52] Abello MC, Gomez MF, Ferretti O. Mo/ $\gamma$ -Al<sub>2</sub>O<sub>3</sub> catalysts for the oxidative dehydrogenation of propane. Effect of Mo loading. *Appl Catal A – Gen* 2001;207(1–2):421–31.
- [53] Qin SD, Zhang CH, Xu J, Wu BS, Xiang HW, Li YW. Effect of Mo addition on precipitated Fe catalysts for Fischer–Tropsch synthesis. *J Mol Catal A – Chem* 2009;304(1–2):128–34.
- [54] Wang B, Yang Y, Li LJ, Chen Y. Effect of different catalyst supports on the (n,m) selective growth of single-walled carbon nanotube from Co–Mo catalyst. *J Mater Sci* 2009;44(12):3285–95.
- [55] Munteanu G, Ilieva L, Andreeva D. Kinetic parameters obtained from TPR data for  $\alpha$ -Fe<sub>2</sub>O<sub>3</sub> and Au/ $\alpha$ -Fe<sub>2</sub>O<sub>3</sub> systems. *Thermochim Acta* 1997;291(1–2):171–7.
- [56] Zhang Q, Zhou WP, Qian WZ, Xiang R, Huang JQ, Wang DZ, et al. Synchronous growth of vertically aligned carbon nanotubes with pristine stress in the heterogeneous catalysis process. *J Phys Chem C* 2007;111(40):14638–43.
- [57] Li Y, Zhang XB, Shen LH, Luo JH, Tao XY, Liu F, et al. Controlling the diameters in large-scale synthesis of single-walled carbon nanotubes by catalytic decomposition of CH<sub>4</sub>. *Chem Phys Lett* 2004;398(1–3):276–82.
- [58] Yoshihara N, Ago H, Tsuji M. Chemistry of water-assisted carbon nanotube growth over Fe–Mo/MgO catalyst. *J Phys Chem C* 2007;111(31):11577–82.
- [59] Zhang H, Shin DH, Lee HS, Lee CJ. High-quality single-walled carbon nanotubes synthesized by catalytic decomposition of xylene over Fe–Mo/MgO catalyst and their field emission properties. *J Phys Chem C* 2007;111(35):12954–9.
- [60] Lee TJ, Lee H. Ultraviolet irradiated ozone treatment of a metal catalyst for the large-scale synthesis of single-walled carbon nanotubes with small, uniform diameters. *Carbon* 2008;46(11):1443–9.
- [61] Liu Y, Qian WZ, Zhang Q, Ning GQ, Wen Q, Luo GH, et al. The confined growth of double-walled carbon nanotubes in porous catalysts by chemical vapor deposition. *Carbon* 2008;46(14):1860–8.
- [62] Qian WZ, Wei F, Liu T, Wang ZW, Li YD. What causes the carbon nanotubes collapse in a chemical vapor deposition process. *J Chem Phys* 2003;118(2):878–82.
- [63] Huang JQ, Zhang Q, Xu GH, Qian WZ, Wei F. Substrate morphology induced self-organization into carbon nanotube

- 
- arrays, ropes, and agglomerates. *Nanotechnology* 2008;19(43):435602-1-8.
- [64] Su DS. The use of natural materials in nanocarbon synthesis. *ChemSusChem* 2009;2(11):1009-20.
- [65] Hou PX, Liu C, Cheng HM. Purification of carbon nanotubes. *Carbon* 2008;46(15):2003-25.